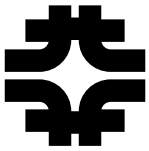

Fermi National Accelerator Laboratory

FERMILAB-Conf-96/272-E
D0

D0 Papers on QCD with Vector Bosons Submitted to DPF '96

D.P. Casey, W. Chen and T. Joffe-Minor
For the D0 Collaboration

Fermi National Accelerator Laboratory
P.O. Box 500, Batavia, Illinois 60510

September 1996

Proceedings of the *American Physical Society Division of Particles and Fields '96*,
Minneapolis, Minnesota, August 10-15, 1996

Disclaimer

Distribution

FERMILAB CONF-96/272-E

DØ PAPERS ON QCD WITH VECTOR BOSONS SUBMITTED TO DPF '96

D.P. Casey, W. Chen, T. Joffe-Minor
for the DØ Collaboration

Contents

p_T DEPENDENCE OF INCLUSIVE Z BOSON PRODUCTION

Dylan P. Casey
for the DØ Collaboration

University of Rochester, Rochester, New York, 14620

We present preliminary results for the measurement of $[1/\sigma]d\sigma/dp_T$ for the Z boson observed in the e^+e^- channel for $p_T < 50$ GeV/c. The data are from a luminosity of ~ 90 pb^{-1} collected with the DØ detector during the 1994–1995 Tevatron run. The differential spectrum is sensitive to non–perturbative predictions of QCD.

1 Introduction

The measurement of the differential p_T distribution for the Z boson provides a sensitive test of the resummation formalism used to describe low–p_T vector boson production. Besides being of interest on its own merits [1], because the uncertainty in the phenomenology of vector boson production contributes 65 MeV to the total uncertainty on M_W [2], a precise measurement of $d\sigma/dp_T$ can also improve the precision in M_W. The Z is chosen over the W for this study because the p_T resolution is significantly better for Z events ($\delta p_T(Z) \sim 1.0$ GeV/c and $\delta p_T(W) \sim 4.0$ GeV/c).

2 Data selection

The data are from the 1994-1995 run of the Tevatron, corresponding to ~ 90 pb^{-1} of total luminosity. For the final data selection, both electron candidates are required to have $E_T > 25$ GeV, $|\eta| \leq 1.1$, and the ϕ of each electron candidate is required to be within the central 90% of the front–surface area of each calorimeter module in order to avoid cracks between the modules. The invariant mass of each Z candidate is restricted to $75 < M_{ee} < 105$ GeV. In addition, both electron candidates are required to be of high quality, *i.e.*, be isolated and have a shower shape consistent with that of an electron, and at least one of the candidates is required to have a charged track pointing to the shower in the calorimeter.

The ultimate goal of the analysis is to obtain an absolute measurement of the differential cross section where detector effects (*e.g.*, smearing in p_T) have been accounted for. For this preliminary result, we account for p_T--dependent efficiency corrections and compare the shape ($[1/\sigma]d\sigma/dp_T$) to resolution–smeared theory.

3 Acceptance and Background

The acceptance defined by the fiducial and kinematic selection criteria varies as a function p_T (Z), and therefore the cross section in each p_T bin must be corrected for this effect. The acceptance is determined on average for each bin using a fast Monte Carlo detector simulator developed for the measurement of the W mass. The most significant distortions of the shape as a function of p_T are from the E_T and η requirements imposed on the data.

The total background level is obtained by fitting the e^+e^- invariant mass spectrum to a Breit–Wigner convoluted with a Gaussian, plus an exponential with fixed slope for the background. The relative normalization of the signal to background is allowed to float. The slope of the background spectrum is determined using dielectron events in which both electron candidates fail the quality criteria for the signal, but pass the same kinematic and fiducial criteria used for the signal. The fitted background level is found to be 2.5%.

The shape of the background as a function of p_T is determined using the same set of failed dielectron events, but with an additional invariant mass requirement of $75 < M_{ee} < 105$ GeV. A simple parameterization was chosen using the function $(p_T + \alpha)e^{\beta p_T}$, where α and β are fit parameters with values $\alpha = 0.99$ and $\beta = -0.125$. The uncertainties in the shape and level of background are conservatively assigned to be 50% for each bin in p_T

4 Results

The cross section in each p_T bin is extracted using the method of statistical inference [3]. The joint posterior probability is obtained using Bayes' Theorem: $P(a_i, b_i, \sigma_i | d_i, I) = P(d_i | a_i, b_i, \sigma_i, I) P(a_i | I) P(b_i | I) P(\sigma_i | I)/Z$, where Z is the normalization requirement, I represents our implicit assumptions and we have assumed that the acceptance (a_i), background (b_i), and the true cross section (σ_i) are logically independent. The likelihood, $P(d_i | a_i, b_i, \sigma_i, I)$, is a Poisson distribution for the data, d_i, given the expected number of events, μ_i, where $\mu_i = L a_i \sigma_i + b_i$ and L is the total luminosity. The priors for the background and acceptance are taken to be Gaussian distributions with the measured value as the mean and the uncertainty as the standard deviation. The prior for the cross section is taken to be flat over $[0, 10] nb$. The final cross section in each bin is obtained by integrating over a_i and b_i, and calculating the first moment. The standard deviation in each bin $(\sqrt{< x^2 > - < x >^2})$ is assigned to be the uncertainty. The preliminary result for $[1/\sigma] d\sigma/dp_T$ is shown in Figure 1. Also shown for comparison is the phenomenology from Ladinsky and Yuan [1], using MRSA structure functions, and smeared with the DØ detector resolutions.

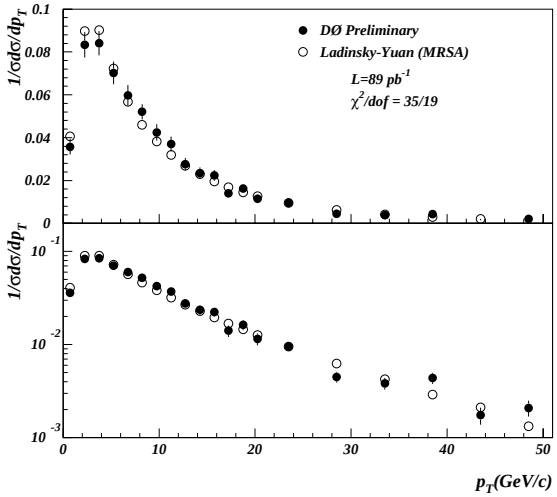

Figure 1: The extracted differential cross section compared to resolution–smeared theory.

In the future, the analysis will include ∼50% more data by including regions of $|\eta| > 1.1$. We expect to reduce the bin size in the region $p_T <$ 15 GeV/c to less than 1.0 GeV/c, improve the systematic errors on the acceptance and background, obtain the unsmeared distribution, and determine an absolute cross section.

References

1. G. Ladinsky and C.P. Yuan, *Phys. Lett.* B **355**, 548 (1995). P. Arnold and R. Kaufman, *Nucl. Phys.* B **349**, 381 (1991). G. Altarelli, R.K. Ellis, M. Greco, and G. Martinelli, *Nucl. Phys.* B **246**, 12 (1984).
2. S.Abachi *et al.*, *FNAL PUB-96/177-E.*
3. E.T.Jaynes, *Probability Theory: The Logic of Science,* unpublished manuscript, http://bayes.wustl.edu. H.Jeffreys, *Theory of Probability*, Clarendon Press, Oxford (1939). R.T.Cox, "Probability, Frequency, and Reasonable Expectation", *Am. Jour. Phys.* **14**, 1 (1946).

ISOLATED PROMPT SINGLE PHOTON AND DIPHOTON PRODUCTION IN $\overline{p}p$ COLLISIONS AT $\sqrt{s} = 1.8$ TeV

WEI CHEN
State University of New York at Stony Brook, NY 11794
The DØ Collaboration, FermiLab

A measurement of the differential cross section $d^2\sigma/dE_{\rm T}d\eta$ of isolated prompt photons, $\overline{\rm p}{\rm p} \to \gamma + {\rm X}$ is presented for two pseudorapidity ranges, $|\eta| < 0.9$ and $1.6 < |\eta| < 2.5$, at $\sqrt{s} = 1.8$ TeV. The data were accumulated during the 1992-1993 tevatron collider run (1A), consisting of 13 pb^{-1} of integrated luminosity. The background is estimated by measuring the longitudinal shower profile in the four layers of the electromagnetic (EM) calorimeter. The results show good agreement with the next-to-leading-order QCD (NLO) calculations in the range $30 \lesssim E_{\rm T} \lesssim 80\,{\rm GeV}$. A preliminary measurement of isolated prompt diphoton production, $\overline{p}p \to \gamma\gamma + X$ is also presented for the pseudorapidity range $|\eta| < 1.0$. The data sample corresponds to an integrated luminosity of 80.0 pb^{-1} from the 1994-1995 run (1B). Preliminary cross section measurements of $d\sigma/dE_{\rm T}$, $d\sigma/dM$ and $(1/\sigma)d\sigma/dK_{\rm T}$ are reported and compared to the Pythia Monte Carlo. The $K_{\rm T}$ (defined as $K_{\rm T} = |\vec{P_T^1} + \vec{P_T^2}|$) of the two photon system is measured in the range $0 < K_{\rm T} < 22\,{\rm GeV}$. The shape at low $K_{\rm T}$ data favors NLO QCD with an intrinsic $\langle K_{\rm T}\rangle = 2\,{\rm GeV}$ rather than the Pythia Monte Carlo or the NLO QCD calculation without an intrinsic $\langle K_{\rm T}\rangle$.

1 Introduction

The production of prompt photons with large transverse momentum in hadronic collisions ($\overline{p}p$) is a clean process to test QCD and extract information about the constituents of the hadron. [1,2] A measurement of the prompt photon cross section has the advantage that the photon transverse energy is not affected by fragmentation and hadronization, resulting in smaller experimental uncertainties than those obtained in jet cross sections. Next-to-leading order QCD calculations are available for both single [3,4] and double photon production [6,7], and can be directly compared to the experimental data.

The *DØ* detector [8] has several features well suited for the detection of prompt photons. The uranium-liquid argon calorimeter has good electromagnetic energy resolution $\sigma_E/E = 13.5\%/\sqrt{E} \oplus 1.4\%$, fine transverse granularity $\Delta\eta \times \Delta\phi = 0.1 \times 0.1$ (0.05×0.05 at shower maximum) and good rϕ and z shower position resolutions. The EM calorimeter has four longitudinal layers segmented as $2 + 2 + 6.8 + 9.8$ radiation lengths. The fine depth segmentation provides a method to distinguish the prompt photons from the background of photon decays of π^0 and η which are copiously produced in jet fragmentation.

The central tracking chamber has high hit-finding and tracking efficiency and good rϕ resolution $\sigma(\mathrm{r}\phi) = 200\mu$m, which is used to find the position of the event vertex and help to reduce the isolated EM jet background.

2 Isolated Prompt Single Photon Production

2.1 Trigger and Event Sample Selection

Prompt photon signals can be distinguished from the overwhelming jet background by selecting local, isolated and well-profiled EM showers in the calorimeter. DØ uses a three-level trigger systems. The first level trigger (level 0) is made of scintillator counters near the beam pipe to detect a $\overline{p}p$ collision. The second level (level 1) is a hardware trigger which makes a fast sum of the EM energy in calorimeter towers ($\Delta\eta \times \Delta\phi = 0.2 \times 0.2$). Photon candidates must have their summed energy above the E_{T} thresholds, which are 2.5, 7.0 and 10.0 GeV. Multiple thresholds are used so that data populate the rapidly-falling E_{T} spectrum over the whole range of 10-125 GeV. The third level (level 2) is a software trigger which performs a fast clustering of calorimeter cells and calculates the cluster's transverse energy, its isolation value, and its longitudinal and transverse shower shape quantities. Shower shape cuts are applied to select photon candidates whose shower shapes are consistent with test beam electrons. The candidate events are further required to satisfy isolation cut. The three level 2 E_{T} thresholds are 6.0, 14.0 and 30.0 GeV respectively.

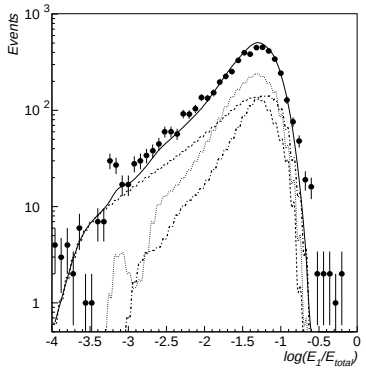

Figure 1: Distribution of $\log(E_{\mathrm{EM1}}/E_{\mathrm{total}})$ for $E_{\mathrm{T}}^{\gamma} = 40 \pm 5\,\mathrm{GeV}$ central photon candidates (solid points), and the fitted distribution (solid curve) made up of Monte Carlo photons (dashes), neutral pions (dots), and η mesons (dot-dash curve). The neutral pion and η meson distributions at small $\log(E_{\mathrm{EM1}}/E_{\mathrm{total}})$ fluctuate due to limited Monte Carlo statistics.

Offline, more sophisticated cuts are applied to photon candidates. Fiducial cuts are applied to restrict candidates to the regions of pseudorapidity $|\eta| < 0.9$ and $1.6 < |\eta| < 2.5$. All candidates are required to be away from the boundary of a central calorimeter module by at least 5% of the module width. No tracks can be found in the road of $\Delta\phi \times \Delta\eta$ between the shower center and the event vertex, where $\Delta\phi = 0.2$ and $\Delta\eta$ is tuned to

the resolution of the shower position along z and the vertex. The EM fraction of the shower must be greater than 96%. The transverse isolation energy, defined as the $E_{\rm T}$ in the cone of $R = 0.4$ minus the $E_{\rm T}$ in the EM core cone of $R = 0.2$ (R = $\sqrt{\Delta\eta^2 + \Delta\phi^2}$), is required to be less than 2.0 GeV. The longitudinal and transverse shower profiles (measured by a 41 $\times$ 41 matrix) must be consistent with those expected for electrons.[9] Having found events with one well-identified, isolated photon, two additional cuts are applied to the whole event that the event z vertex is required to be within 50 cm of the nominal vertex and the missing transverse energy $\not\!\!E_T$ of the event has to be less than 20.0 GeV.

2.2 Background Subtraction

After the above tight event selection cuts, the prompt photon sample still contains a significant background, primarily due to $\gamma\gamma$ decays of π^0 and η when the fluctuations in the jet fragmentation lead to a single meson carrying most of the jet transverse energy. The transverse granularity of the DØ calorimeter is not fine enough to distinguish two γ's ($\pi^0 \to \gamma\gamma$ or $\eta \to \gamma\gamma$) from a single prompt photon at transverse energy $E_{\rm T} > 10\,{\rm GeV}$. But longitudinally two photons from a meson decay are likely to start showering earlier and deposit more energy in the first layer EM1 of the EM calorimeter than a single prompt photon. The distribution of $\log(E_{\rm EM1}/E_{\rm TOTAL})$ is used to estimate the fraction of candidate events which are true photons. (see fig. 1) We assume the data are composed of true prompt photons and meson backgrounds (π^0 and η). Fitting to the distributions of $\log(E_{\rm EM1}/E_{\rm TOTAL})$ at several $E_{\rm T}$ points results in an $\rm E_T$ dependent photon purity, $\mathcal{P}$, with an exponential form $\mathcal{P} = 1 - e^{-(a+b*E_{\rm T})}$.

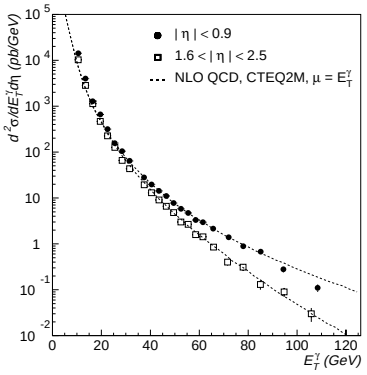

Figure 2: The inclusive isolated prompt photon cross section $\sigma_e = d^2\sigma/dE_{\rm T}^{\gamma}d\eta$ as a function of photon transverse energy $E_{\rm T}^{\gamma}$, for central (circles) and forward regions (squares). The errors are statistical only. The NLO QCD calculated cross sections $\sigma_{\rm t}$, using CTEQ2M parton distributions with $\mu = E_{\rm T}^{\gamma}$, are shown for comparison.

2.3 Inclusive Single Photon Cross Section

The differential cross section $d^2\sigma/dE_{\rm T}d\eta$ for inclusive isolated prompt photon production is shown in fig. 2, using a data set of 13 pb^{-1} of integrated luminosity (1A). The data are compared to next-to-leading-order QCD calculations [3] with CTEQ2M parton distribution function and renormalization scale $\mu = E_{\rm T}$. Fig. 3 plots $(\sigma_{\rm e} - \sigma_{\rm t})/\sigma_{\rm t}$ where $\sigma_{\rm e}$ and $\sigma_{\rm t}$ are the experimental and theoretical values respectively. The experimental cross sections are in good agreement with NLO QCD for both pseudorapidity regions for the range $30 < E_{\rm T} < 80\,{\rm GeV}$. At the low transverse energy $E_{\rm T} < 20\,{\rm GeV}$, the data show an excess over the NLO QCD prediction. At the high transverse energy $E_{\rm T} > 74\,{\rm GeV}$, the data for the central region lie below the QCD calculations, which is within the experimental uncertainties.

3 Isolated Prompt Double Photon Production

3.1 Data Sample and Efficiencies

Just as in the single photon analysis, prompt diphoton signals can be distinguished from the background of γ+"jet" and "jet"+"jet" by selecting isolated EM showers in the calorimeter. The diphoton candidates are taken when two or more level 1 EM trigger towers pass an $E_{\rm T}$ threshold of 7 GeV. In the level 2 trigger, they must have at least two clusters with $E_{\rm T}$ greater than 12 GeV, a longitudinal and transverse shower shape consistent with test beam electrons for both clusters, and one cluster has to be isolated.

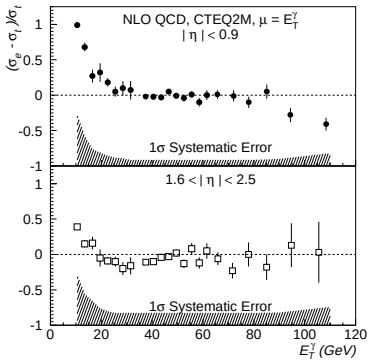

Figure 3: Difference between the measured isolated photon cross section $\sigma_{\rm e}$ and the NLO QCD prediction $\sigma_{\rm t}$, normalized to the latter. The shaded bands show the magnitude of the combined experimental systematic errors $(1\,\sigma)$ for each of the two regions.

Rather low $E_{\rm T}$ cuts are used offline to preserve good statistics. It becomes important to understand the $E_{\rm T}$ dependent trigger efficiencies and offline cuts efficiencies. The trigger efficiencies in the range $E_{\rm T} < 25$ GeV are measured by using special run data with lower trigger thresholds. The efficiencies in the range $E_{\rm T} > 25$ GeV are determined using an inclusive $Z \to ee$ sample. The whole $E_{\rm T}$ dependent efficiency curve is shown in fig. 4 (a).

The diphoton sample is then streamed through "loose" photon ID cuts, which results in a "clean" sample of 3477 candidates. The "clean" sample was re-reconstructed using the latest reconstruction package. The final candidate sample is selected by applying "tight" photon ID cuts, which results in 418 remaining events.

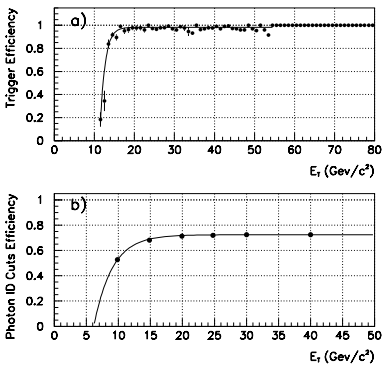

Figure 4: (a) The trigger efficiency per photon as a function of the photon transverse energy for the diphoton trigger. (b) The combined photon ID cuts efficiency per photon vs. the photon $E_{\rm T}$. The shape is measured by developing a detailed simulation of the showers of electrons and photons in the calorimeter with overlaid minimum bias events to model the calorimeter noise and underlying events. The normalization is determined from data.

The "tight" photon ID cuts include the fiducial cuts, which are $|\eta| < 1.0$ and ϕ position being away from the boundary of a central calorimeter module by at least 5% of the module width, and the kinematic cuts, which are $E_{\rm T}^1 > 14\,{\rm GeV}$ and $E_{\rm T}^2 > 13\,{\rm GeV}$. Each photon must satisfy the following quality cuts. No tracks can be found in the road (as in the single photon analysis), the EM fraction be greater than 90%, the isolation transverse energy $E_{\rm T} < 2\,{\rm GeV}$, the tight longitudinal and transverse shower profile cut[9], and the central tracking cuts which require the ratio of CDC hit wires to total wires to be less than 0.85 and no CDC hits have z position information. The $E_{\rm T}$ dependent efficiency of the offline cuts is shown in Fig. 4 (b).

A large Pythia[5] Monte Carlo sample (2 million events) was generated to study the geometric acceptance of the diphoton events. The acceptance values are flat over a large range of $E_{\rm T}$ of each photon and the mass, the $K_{\rm T}$ and the $\Delta\phi$ of the diphoton system. The average geometric acceptance is 0.688 ± 0.002.

3.2 Background Evaluation

A method similar to that used in the single prompt photon analysis was developed to estimate the diphoton background. Instead of fitting to the whole distribution of $log(E_{\rm EM1}/E_{\rm Total})$, a simple exponential function $e^{A-B*E_{\rm T}}$ fit is performed to the central region of the distributions (see Fig. 5). The distribution of the data is fitted as a sum of the distributions of photon, π^0 and η. The diphoton candidate sample is divided into three subsamples, $E_{\rm T}^1 < 20\,{\rm GeV}$ and $E_{\rm T}^2 < 20\,{\rm GeV}$, $E_{\rm T}^1 > 20\,{\rm GeV}$ and $E_{\rm T}^2 < 20\,{\rm GeV}$, and $E_{\rm T}^1 > 20\,{\rm GeV}$ and

Subsamples	$\alpha_{\gamma\gamma}$
$E_{\rm T}^1 < 20, E_{\rm T}^2 < 20$	0.257 ± 0.095
$E_{\rm T}^1 > 20, E_{\rm T}^2 < 20$	0.301 ± 0.112
$E_{\rm T}^1 > 20, E_{\rm T}^2 > 20$	0.375 ± 0.227

Table 1: Evaluated purity $\alpha_{\gamma\gamma}$

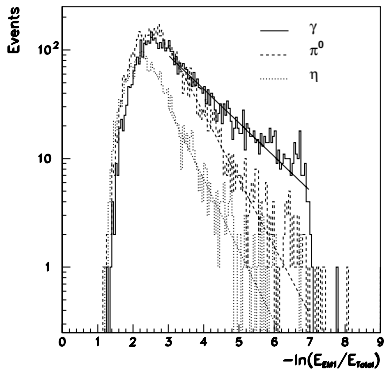

Figure 5: Distribution of $\ln(E_{\rm EM1}/E_{\rm total})$ for $E_{\rm T} = 20\,{\rm GeV}$ of γ, π^0 and η respectively. A simple exponential function fit is shown for each curve.

$E_{\rm T}^2 > 20\,{\rm GeV}$. Table 1 lists the fitted purity $\alpha_{\gamma\gamma}$ for the three subsamples.

3.3 Cross Section Measurements and Comparison with QCD

The differential cross sections $d\sigma/dE_{\rm T}$ and $d\sigma/d{\rm M}$ for inclusive isolated prompt diphoton production, using a data set of 80 pb^{-1} of $p\overline{p}$ collisions during the 1994-1995 run (1B), are shown in Figure 6(a). A Pythia Monte Carlo program is developed to compare to the data. It uses the CTEQ2M parton distribution functions and smears the kinematic values of a photon with calorimeter energy and angular resolutions.

For the two photon system, $K_{\rm T}$ is defined as $|\vec{P_T^1} + \vec{P_T^2}|$. At leading order QCD, $d\sigma/dK_{\rm T}$ peaks at $K_{\rm T} = 0$. Only next-to-leading order (or higher order) QCD gives the two photon system a $P_{\rm T}$ push which results in a shift of the peak of $d\sigma/dK_{\rm T}$ to a nonzero value. The distribution of $d\sigma/dK_{\rm T}$ is therefore a good test of higher-order QCD. Figure 6(b) shows a normalized distribution $(1/\sigma)d\sigma/dK_{\rm T}$ for the data, the Pythia monte carlo, the NLO QCD calculation[6] and the NLO QCD calculation with an additional $\langle K_{\rm T}\rangle = 2\,{\rm GeV}$. The NLO QCD calculation with an additional $\langle K_{\rm T}\rangle = 2\,{\rm GeV}$ describes the data the

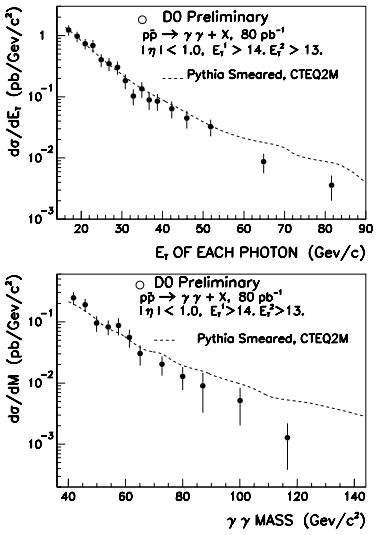

(a) The inclusive isolated prompt diphoton cross sections $d\sigma/dE_{\rm T}$ vs. $E_{\rm T}$ of each photon (the upper) and $d\sigma/d$M vs. mass of $\gamma\gamma$ (the lower). The Pythia monte carlo is shown for comparison.

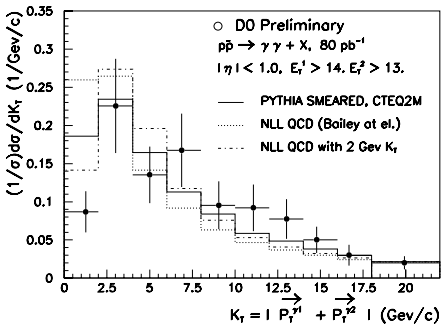

(b) The normalized cross section $(1/\sigma)d\sigma/dK_{\rm T}$ vs. $K_{\rm T}$ in the range $0 < K_{\rm T} < 22\,$GeV. It is compared to the pythia MC, the NLO QCD and the NLO QCD with $\langle K_{\rm T}\rangle = 2\,$GeV.

better at the low $K_{\rm T}$.

References

1. J.F.Owen, *Rev. of Modern Phys.* **59**, 465 (1987)
2. T.Ferbel and W.R.Molzon, *Rev. of Modern Phys.* **56**, 181 (1984)
3. J.Ohnemus,H.Baer and J.F.Owens, *Phys. Rev.* D **42**, 61 (1990)
4. P.Aurenche *etal.*, *Nucl. Phys.* B **297**, 661 (1988)
5. Pythia 5.7, described by T.Sjostrand in *Comput. Phys. Commun.* **82**, 74 (1994)
6. B.Bailey and J.F.Owens, *Phys. Rev.* D **46**, 2018 (1992)
7. P.Aurenche *etal.*, *Z. Phys.* C **29**, 459 (1985)
8. S.Abachi *etal.*, *Nucl. Instrum. Methods* A **338**, 185 (1994)

9. For more details, see S.Abachi *etal.*, *Phys. Rev.* D **52**, 4877 (1995)

A MEASUREMENT OF THE RATIO OF $W + 1$ Jet TO $W + 0$ Jets CROSS SECTIONS AND COMPARISONS TO QCD

TACY JOFFE-MINOR
Northwestern University
for the DØ Collaboration

A preliminary measurement of the ratio, $\mathcal{R}^{10}$, of the production cross sections for $W + 1$ Jet and $W + 0$ Jets processes at a center of mass energy, $\sqrt{s}$, of 1800 GeV by the DØ Collaboration is presented. A comparison of this ratio is made to next-to-leading order, NLO, calculations and the implications of these comparisons, especially for the extraction of a value for the strong coupling constant $\alpha_S(M_W^2)$, are discussed.

The UA1 and UA2 experiments[1,2] used $W(\rightarrow e\nu)+$ Jets to measure the ratio, $\mathcal{R}^{10}$, of the production cross sections for $W + 1$ Jet events to $W + 0$ Jets events and then used theoretical calculations to extract a value for $\alpha_S(M_W^2)$. The DØ collaboration has also published[3] a measurement of the ratio of production cross sections using the data from the 1992-1993 run of the Fermilab Tevatron Collider. The preliminary result presented here is from the 1994–1995 run and uses a data set more than six times as large as that used for the previous DØ result.

The DØ detector and the details of the DØ triggering system have been described elsewhere.[5]

The data sample used for this study is defined offline by selecting $W\rightarrow e\nu$ candidates without a cut on the jet multiplicity. The cuts on the electron include a transverse energy, E_T, cut of 25 GeV, and several quality cuts. The missing E_T, $\not\!\!E_T$, in the event is also required to be greater than 25 GeV. Jets in these events are identified using a fixed cone algorithm with a radius of 0.7 in η–ϕ space. The analysis has been performed using several different minimum E_T, E_T^{min}, requirements used to define the jets. The standard value is chosen to be 25 GeV.

Backgrounds due to multi-jet events, which are the dominant background, are estimated using data. The backgrounds due to Drell–Yan, $Z\rightarrow e^+e^-$ and $Z\rightarrow\tau\tau$ events is estimated using the ISAJET[6] Monte Carlo.

For 75.9 pb^{-1} of data from the 1994-1995 run we obtain 36,891 $W\rightarrow e\nu$ candidates with electrons restricted to the central part of the DØ calorimeter ($|\eta|$ <1.1). For a cut on E_T^{min} of 25 GeV there are 33,511 $W + 0$ Jets candidates and 2,841 $W + 1$ Jet candidates. After subtracting the background contributions from multi-jet events and from other electroweak processes these numbers become 32,835 for $W + 0$ Jets and 2,599 for $W + 1$ Jet. This results

in a ratio of

$$\mathcal{R}^{10}_{exp}(\boldsymbol{preliminary}) = 0.079 \pm 0.002^{stat} \pm 0.005^{sys}.$$

The dominant systematic error is due to the uncertainty in the jet energy scale.

A comparison of this result with theoretical calculations (Figure 1) using the DYRAD [4], a NLO QCD prediction, and the CTEQ3 [7] family of parton distribution functions, pdf, in which the distributions were refit for several fixed values of Λ_{QCD}, shows that not only is the prediction significantly below the experimental result, but the calculations also exhibit little dependence on α_S making an extraction of α_S by this method impossible.

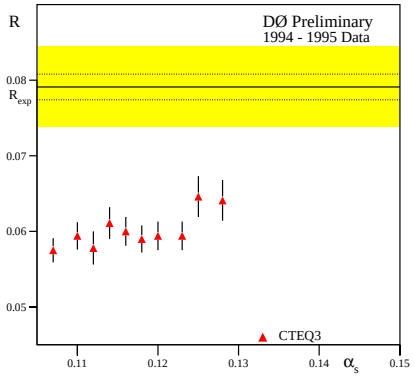

Figure 1: The ratio, $\mathcal{R}^{10}$, for $E_T^{min} = 25$ GeV. The experimental result is the solid line. Dotted lines indicate the statistical errors and the shaded region represents statistical and systematic errors added in quadrature. The points are DYRAD calculations using the CTEQ3 pdf family.

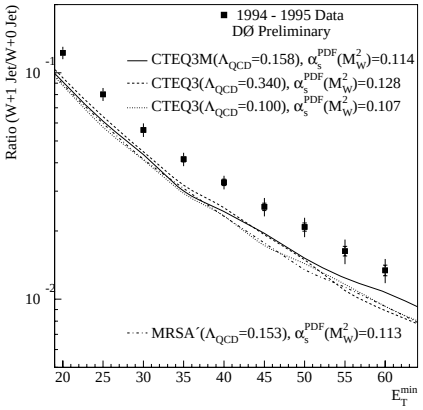

Figure 2: The ratio, $\mathcal{R}^{10}$, decreases as E_T^{min} is increased. Inner error bars are statistical, outer error bars are statistical and systematic added in quadrature. The solid curve is for the preferred CTEQ3M parton distribution functions and the other CTEQ3 curves span the extremes in α_S.

One can also vary E_T^{min} and compare the experimental trend to that of the theoretical predictions (see Figure 2). The theoretical predictions describe the shape of the E_T^{min} dependence for the different parton distribution functions, however all are consistently below the data.

A comparison of the theoretical calculations for DØ to those for UA1/UA2 points to a fundamental difference between the experiments, the center of mass energy of the collisions. Because UA1/UA2 ran at a lower $\sqrt{s}$ than DØ, the average momentum fraction of the initial state partons was larger than the average momentum fraction of the initial partons for W production at DØ. This

difference results in more of the DØ $W + 1$ Jet events being produced from a quark-gluon initial state than the $W + 1$ Jet events at UA1/UA2.[8] Theoretical predictions for $\mathcal{R}^{10}$ at DØ are therefore more sensitive to the gluon distribution in the proton.

The gluon distribution is not well constrained by current experiments. When the CTEQ3 pdf's are plotted for the different partons in the proton it can be seen that the gluon distribution changes significantly as Λ_{QCD} is varied. This variation contributes to the flattening of the theoretical predictions for $\mathcal{R}^{10}$ *vs.* α_s by compensating for the changes in the matrix element as α_s increases.

In conclusion, DØ has made a preliminary measurement of the ratio of production cross sections for $W + 1$ Jet to $W + 0$ Jets processes with the data from the 1994-1995 run of the Fermilab Tevatron Collider. Comparisons to NLO QCD calculations show that the theoretical predictions are consistently lower than the data for different values of α_s given the currently available parton distribution functions. Also, the theoretical calculations underestimate the rate of jet production in association with W bosons as a function of the minimum jet E_T. It appears that incorporating the DØ and the UA1/UA2 data in global QCD fits could lead to modifications of the conventional understanding of the gluon distribution in the proton.

We acknowledge the support of the US Department of Energy and the collaborating institutions and their funding agencies in this work. We express our appreciation to W.T. Giele for providing modifications to the theoretical predictions appropriate to this measurement.

References

1. UA1 Collaboration, M. Lindgren *et al. Phys. Rev.* D **45**, 3038 (1992)
2. UA2 Collaboration, J. Alitti *et al. Phys. Lett.* B **263**, 563 (1991)
3. S. Abachi *et al. Phys. Rev. Lett.* **75**, 3226 (1995)
4. W.T. Geile, E.W.N. Glover and D.A. Kosower, *Nucl. Phys.* B **403**, 633 (1993)
5. S. Abachi *et al. Nucl. Instrum. Methods* A **338**, 185 (1994)
6. F. E. Paige and S. D. Protopopescu,"ISAJET Manual", Brookhaven National Laboratory, Upton, New York (1992)
7. CTEQ Collaboration, H. L. Lai *et al. Phys. Rev.* D **51**, 4763 (1995)
8. F. A. Berends, W. T. Giele, H. Kuijf, R. Kleiss and W. J. Stirling, *Phys. Lett.* B **224**, 237 (1989)